ChemPubSoc Europe

DOI: 10.1002/chem.201604921

CHEMISTRY
A European Journal
Full Paper

Supramolecular Chemistry

Complexation and Electronic Communication between Corannulene-Based Buckybowls and a Curved Truxene-TTF Donor

María Gallego+,[a] Joaquín Calbo+,[b] Rafael M. Krick Calderon+,[c] Paula Pla,[b] Ya-Chu Hsieh,[d] Emilio M. Pérez,[e] Yao-Ting Wu,*[d] Enrique Ortí,*[b] Dirk M. Guldi,*[c] and Nazario Martín*[a, e]

Dedicated to the memory of Prof. José Barluenga for his outstanding contributions to the progress of science in Spain

Abstract: The association behavior of an electron-donating, bowl-shaped, truxene-based tetrathiafulvalene (truxTTF) with two corannulene-based fullerene fragments, $C_{32}H_{12}$ and $C_{38}H_{14}$, is investigated in several solvents. Formation of 1:1 complexes is followed by absorption titrations and complemented by density functional theory (DFT) calculations. The binding constants are in the range $\log K_a = 2.9–3.5$. DFT calculations reveal that the most stable arrangement is the conformation in which the 1,3-dithiole ring of truxTTF is placed inside the concave cavity of the corannulene derivative. This arrangement is confirmed experimentally by NMR measurements, and implies that a combination of π–π and CH–π interactions is the driving force for association. Time-dependent DFT calculations reproduce the experimental UV/Vis titrations and provide a detailed understanding of the spectral changes observed. Femtosecond transient absorption studies reveal the processes occurring after photoexcitation of either $C_{32}H_{12}$ or $C_{38}H_{14}$ and their supramolecular associates with truxTTF. In the case of truxTTF·$C_{38}H_{14}$, photoexcitation yields the charge-separated state truxTTF$^{\bullet+}$·$C_{38}H_{14}^{\bullet-}$ with a lifetime of approximately 160 ps.

Introduction

Polycyclic aromatic hydrocarbons (PAHs) represent a large family of molecular building blocks based on multiple fused aromatic rings.[1–3] If PAHs are formed solely by fused benzene rings, their structure remains planar, except in helicenes[4–6] or highly strained cyclic derivatives,[7–11] whereas PAHs featuring five-membered rings as part of their structure adopt nonplanar equilibrium geometries. In an extreme scenario, spherical fullerenes evolve upon embedding twelve five-membered rings into a PAH structure. Notably, any number of five-membered rings below twelve produces bowl-shaped molecules, or "buckybowls".[12,13]

The fact that the concave and convex surfaces of buckybowls, on one hand, and their edges, on the other hand, are readily available for reactions offers intriguing possibilities in chemistry. The convex surface often shows reactivity patterns similar to those seen for fullerenes. For example, upon treatment of $C_{26}H_{12}$, the smallest fullerene fragment featuring a [6,6] double bond, under the conditions for 1,3-dipolar cycloaddition, carbine addition, or nucleophilic addition of MeLi, it exhibits reactions as found for [60]fullerene, that is, addition reactions at the central [6,6] ring junction. If it is subjected to Friedel–Crafts alkylation conditions, $C_{26}H_{12}$ behaves like an ordinary PAH, that is, it reacts at the double bonds located at the edges.[14] A more complex scenario occurs if more than one type of [6,6] double bond is present in the buckybowl. For example, for the larger circumtrindene ($C_{36}H_{12}$)[15] under 1,3-dipolar cycloaddition conditions, the process is site-selective for [6,6] bonds located at the point of greatest curvature.[14] This chemical reactivity resembles that observed for C_{70}. C_{70} shows five types of [6,6] bonds, but only the α and β isomers are typically detected under Prato reaction conditions, with a large preference for the α isomer. In some rare cases, traces of the γ isomer are also observed.[16]

[a] Dr. M. Gallego,+ Prof. Dr. N. Martín
Departamento de Química Orgánica, Fac. C. C. Químicas
Universidad Complutense de Madrid, Av. Complutense s/n
28040 Madrid (Spain)
E-mail: nazmar@ucm.es

[b] J. Calbo,+ P. Pla, Prof. Dr. E. Ortí
Instituto de Ciencia Molecular, Universidad de Valencia
46980 Paterna (Spain)
E-mail: enrique.orti@uv.es

[c] Dr. R. M. Krick Calderon,+ Prof. Dr. D. M. Guldi
Department of Chemistry and Pharmacy and Interdisciplinary Center for Molecular Materials (ICMM), Friedrich-Alexander-Universität
Erlangen-Nürnberg, 91058 Erlangen (Germany)
E-mail: dirk.guldi@fau.de

[d] Dr. Y.-C. Hsieh, Prof. Dr. Y.-T. Wu
Department of Chemistry, National Cheng Kung University
70101 Tainan (Taiwan)
E-mail: ytwuchem@mail.ncku.edu.tw

[e] Dr. E. M. Pérez, Prof. Dr. N. Martín
IMDEA Nanociencia, Faraday 9, Campus UAM, 28049 Madrid (Spain)

[+] These authors contributed equally to this work.

Supporting information and the ORCID identification number for the author of this article can be found under http://dx.doi.org/10.1002/chem.201604921.

Buckybowls also show very rich coordination chemistry, which may occur at either the concave or the convex face, yielding *endo* and *exo* complexes, respectively.[17] The first structurally characterized corannulene complex was $[(Cp^*Ru)_2\mu^2\text{-}\eta^6, \eta^6\text{-}C_{20}H_{10})]^{2+}$, reported by Rabideau and coworkers.[18] To this end, two $(Cp^*Ru)^+$ are bound to nonadjacent arene rings on opposite sides of the corannulene. Notably, η^6-coordination causes reduction of the curvature, and in turn, a flattening of the corannulene. Concave-selective coordination is also possible, with $[CpFe(sumanene)]^+$ the first reported example.[19]

Buckybowls have been targeted as molecular building blocks toward more complex carbon nanoforms such as carbon nanotubes.[20] In particular, buckybowls serve as seeds from which carbon nanotubes of a specific chirality are grown.[21] Finally, and most importantly, buckybowls show unique electronic properties, often in between those of flat PAHs and fullerenes, which can be skillfully exploited for organic electronics applications.[22,23]

With regard to supramolecular chemistry, buckybowls have been studied thoroughly as hosts for fullerenes owing to their shape complementarity.[24–26] However, the association of buckybowls by other organic hosts has hardly been investigated. Recently, we described the association of a fullerene fragment, hemifullerene $C_{30}H_{12}$, by an electron-donating, bowl-shaped tetrathiafulvalene derivative (truxTTF), in which three 1,3-dithiole rings are attached to a truxene core (Scheme 1).[27] The

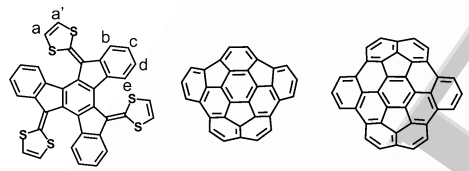

Scheme 1. Chemical structures of truxTTF, $C_{32}H_{12}$, and $C_{38}H_{14}$.

stability of the associate was remarkable, with an association constant of $\log K_a = 3.6 \pm 0.3$ in $CHCl_3$ at room temperature. Moreover, we demonstrated photoinduced electron transfer from truxTTF to $C_{30}H_{12}$ to form the fully charge-separated species, which constituted the first example in which a buckybowl mimicked the electron-accepting properties of fullerenes within supramolecular complexes.[27]

In contrast to hemifullerene $C_{30}H_{12}$, the recently reported larger $C_{32}H_{12}$ and $C_{38}H_{14}$ buckybowls (Scheme 1) are corannulene-based fragments of [60] and [70]fullerene, respectively.[28,29] Such a difference in core aromatic structure is likely to be accompanied by fundamental differences in electronic properties.

Here, we demonstrate that truxTTF forms heteromolecular associates ($\log K_a \approx 3$) with $C_{32}H_{12}$ and $C_{38}H_{14}$ in a variety of organic solvents. Density functional theory (DFT) calculations showed several different approximations of the heteromolecular complexes, all with favorable interaction energies, but only one, that is, the staggered arrangement, with a significant negative free energy of complexation. NMR experiments confirmed the formation of staggered structures for both heterodimers in solution. Spectroelectrochemical and transient absorption studies revealed that photoinduced electron transfer (PET) occurs in truxTTF·$C_{38}H_{14}$, thus showing that corannulene π-extended derivatives resemble the electronic behavior of [60]fullerene.

Results and Discussion

The synthesis and comprehensive characterization of truxTTF,[30] $C_{32}H_{12}$,[31] and $C_{38}H_{14}$[28,29] have been reported elsewhere. Very briefly, truxTTF was synthesized from commercially available truxenone through a threefold Horner–Wadsworth–Emmons olefination with the appropriate■■ok?■■ dithiole phosphonate ilyde. The highly strained $C_{32}H_{12}$ and $C_{38}H_{14}$ were synthesized from the appropriate■■ok?■■ planar fluoranthene derivatives through Pd-catalyzed C–C coupling reactions.

On the basis of our previous experience with hemifullerene $C_{30}H_{12}$, we expected the larger $C_{32}H_{12}$ and $C_{38}H_{14}$ to associate with truxTTF in a similar fashion. To test this hypothesis, we began by investigating the supramolecular interaction in silico, through dispersion-corrected DFT calculations. There are four different ways in which truxTTF and $C_{32}H_{12}$ can interact with each other. These four-modeled configurations are depicted in Figure 1.

In **1** and **2**, the convex surface of $C_{32}H_{12}$ perfectly matches the two concave cavities of the truxTTF host, in particular, either through the cavity formed by the truxene core (structure **1**) or through the cavity formed by the three 1,3-dithiole rings and the central benzene ring of the truxene core (structure **2**). Both are best described as bowl-in-bowl arrangements, in which π–π interactions are maximized. The concave cavities of truxTTF and $C_{32}H_{12}$ can also interact, giving rise to heterodimers in which either a benzene or a dithiole ring of truxTTF is placed inside the concave cavity of the corannulene-based bowl, resulting in **3** and **4**, respectively. These two dispositions resemble the arrangement found in the crystal packing for the homodimers of truxTTF and the related $C_{30}H_{12}$, implying a mixture of π–π and CH–π interactions.[30,32] All the optimized heterodimeric structures (**1**–**4**) show close intermolecular contacts in the 2.5–3.7 Å range (Figure S1 in the Supporting Information), indicative of stabilizing noncovalent interactions between both bowls.

To assess the strength of the interaction between the truxTTF and $C_{32}H_{12}$ bowls, we calculated the association energies for the previously optimized heterodimers at the revPBE0-D3/cc-pVTZ level of theory, including the three-body correction (E_{ABC}) to the dispersion interaction (see Supporting Information for full computational details). **1**–**4** exhibit significant gas-phase association energies ranging from −20.4 and −20.0 kcal mol^{-1} for **1** and **2**, respectively, to −24.7 and −29.9 kcal mol^{-1} for **3** and **4**, respectively (Table 1). The bowl-in-bowl structures are therefore significantly less stable than the staggered arrangements.

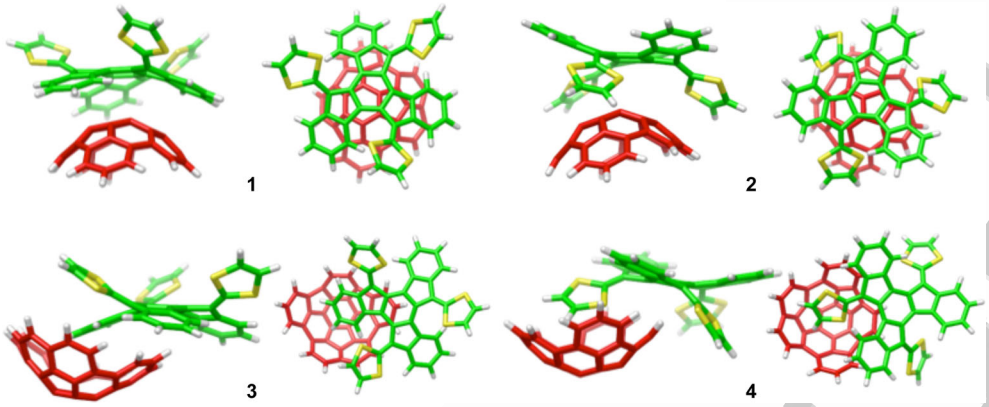

Figure 1. Minimum-energy structures (**1**–**4**) computed at the revPBE0-D3/cc-pVTZ level for the most stable conformations of the heterodimer formed by the $C_{32}H_{12}$ fullerene fragment with truxTTF (truxTTF·$C_{32}H_{12}$). Carbon atoms of the truxTTF are depicted in green, sulfur in yellow, and hydrogen in white. Carbon atoms of $C_{32}H_{12}$ are depicted in red, and hydrogen in white.

Table 1. Thermodynamic parameters [kcal mol^{-1}] including association energy (E_{assoc}), free energy in gas phase (ΔG_{gas}) and free energy including solvent effects (ΔG_{theor}) for the dimerization process. Theoretical and experimental log K_a values are also included.

Heterodimer		E_{assoc}	ΔG_{gas}[b]	ΔG_{theor}[c]	log $K_{a\,theor}$[d]	log $K_{a\,exp}$
truxTTF·$C_{30}H_{12}$[a]	**1′**	−21.02	−8.27	1.13	3.7	3.6 ± 0.3[e]
	2′	−19.38	−5.98	2.64		
	3′	−25.23	−10.88	−2.96		
	4′	−28.52	−14.34	**−5.00**		
truxTTF·$C_{32}H_{12}$	**1**	−20.44	−3.87	5.07	3.2	2.9 ± 0.4[e]
	2	−19.97	−4.24	3.67		3.2 ± 0.1[f]
	3	−24.69	−6.95	0.97		3.3 ± 0.2[g]
	4	−29.91	−12.84	**−4.29**		
truxTTF·$C_{38}H_{14}$	**5**	−23.37	−4.32	5.81	3.6	3.4 ± 0.1[f]
	6	−21.63	−3.46	4.80		
	7	−29.09	−9.72	0.51		
	8	−33.48	−14.39	−3.75		3.5 ± 0.2[g]
	9	−31.57	−11.71	−2.65		
	10	−34.24	−14.94	**−4.93**		

[a] Minimum-energy geometries as used in reference [27]. Notation **1′**–**4′** refers to systems **1**–**4** in the original work. [b] Free energy of complexation including zero-point energy, thermal, enthalpy, and entropy corrections. [c] Free energy of complexation after addition of solvent effects through SMD and chloroform as a solvent. [d] Theoretical log K_a values calculated for the most stable conformer using the ΔG_{theor} value. [e] Determined in $CHCl_3$ as solvent. [f] PhCl as solvent. [g] THF as solvent.

The supramolecular complexes formed by truxTTF and $C_{38}H_{14}$ were likewise modeled in several conformations. Depending on the relative disposition of one moiety with respect to the other, two bowl-in-bowl (**5** and **6**) and four staggered (**7**–**10**) conformations were optimized at the revPBE0-D3/cc-pVTZ level of theory (Figure 2). Conformations **7** and **8** differ from **9** and **10** in an approximately 90° rotation of the staggered arrangements. The bowl-in-bowl arrangements **5** and **6** offer an optimal disposition for maximizing π–π interactions, with short intermolecular contacts in the 3.2–3.8 Å range (Figure S2, Supporting Information). The staggered arrangements **7**–**10** are governed by a mixture of π–π and CH–π interactions between the electron-donating truxTTF and the electron-accepting $C_{38}H_{14}$, with short intermolecular contacts in the range 2.7–3.9 Å (Figure S2).

The bowl-in-bowl arrangements, in which the convex surface of $C_{38}H_{14}$ perfectly matches the two concave cavities of the truxTTF host, are represented in **5** and **6**. Both **5**, through the cavity formed by the carbon backbone, and **6**, through the cavity formed by the central benzene ring and the three dithiole rings, show favorable interactions with stabilizations of −23.4 and −21.6 kcal mol^{-1}, respectively. The staggered arrangements **7**–**10** show significantly larger interaction energies. The conformer in which a dithiole ring of truxTTF is placed inside the concave cavity of $C_{38}H_{14}$ is computed to be the most stable arrangement, with −33.5 kcal mol^{-1} for **8** and −34.2 kcal mol^{-1} for **10** (Table 1).

The interaction energy computed for the most stable structures of heterodimers truxTTF·$C_{32}H_{12}$ and truxTTF·$C_{38}H_{14}$ surpasses the association energy computed for the hemifullerene-truxTTF (truxTTF·$C_{30}H_{12}$) heterodimer (−28.5 kcal mol^{-1}) at the same level of theory.[27] Theoretical calculations therefore suggest favorable arrangements in which truxTTF is merged with corannulene-based $C_{32}H_{12}$ and $C_{38}H_{14}$ carbon nanoforms in highly stable supramolecular heterodimers.

To provide a more realistic description reflecting the strength of complexation at room temperature and in solution, we made theoretical estimations of the free energy of the dimerization process for all the possible conformers of truxTTF·$C_{32}H_{12}$ and truxTTF·$C_{38}H_{14}$, and compared them with that computed for truxTTF·$C_{30}H_{12}$ (see Supporting Information for full computational details). The free energies in the gas phase show that entropic effects are similar for both bowl-in-bowl and staggered dimers (Table S1, Supporting Information). Upon inclusion of solvent effects (chloroform), the ΔG_{theor} values obtained indicate the same trends for the relative stabilities of the different supramolecular arrangements as predicted by the association energy (Table 1). Interestingly, only the staggered conformers provide negative values of ΔG_{theor}, suggesting that bowl-in-bowl arrangements might not be formed in solution (Table 1). For the three buckybowls, the staggered dimers in which the dithiole ring is placed inside the bowl

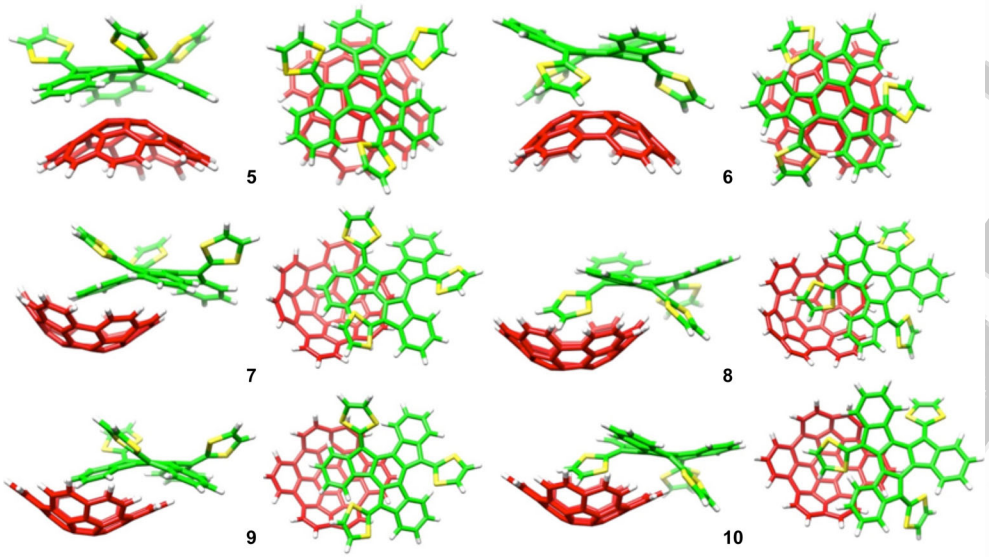

Figure 2. Minimum-energy structures (**5**–**10**) computed at the revPBE0-D3/cc-pVTZ level for the most stable conformations of the heterodimer formed by the $C_{38}H_{14}$ fullerene fragment with truxTTF (truxTTF·$C_{38}H_{14}$). Carbon atoms of the truxTTF are depicted in green, sulfur in yellow, and hydrogen in white. Carbon atoms of $C_{38}H_{14}$ are depicted in red, and hydrogen in white.

basin are computed as the most stable structures, with ΔG_{theor} values of −4.29, −4.93, and −5.00 kcal mol^{-1} for truxTTF·$C_{32}H_{12}$, truxTTF·$C_{38}H_{14}$, and truxTTF·$C_{30}H_{12}$, respectively. Theoretical log K_a values are predicted in the range 3–4, showing a perfect match in the case of truxTTF·$C_{30}H_{12}$ ($\log K_{a,theor} = 3.7$) with respect to the experimental value ($\log K_{a,exp} = 3.6 \pm 0.3$) reported previously.[27] Calculations using chlorobenzene led to both qualitatively and quantitatively similar results (Table S1, Supporting Information).

Considering these encouraging results, we studied the association in solution through absorption titrations in PhCl, $CHCl_3$, and THF at room temperature. Typical results for the titration of truxTTF with $C_{32}H_{12}$ are shown in Figure 3a. Overall, the spectral changes are very small. For example, the truxTTF band at 450 nm lacks any notable decrease in absorption despite the fact that $C_{32}H_{12}$ absorbs only very weakly in this spectral region.[28] However, a very weak increase in absorption in the 500–600 nm region was observed, which is correctly reproduced by TDDFT calculations (vide infra) and parallels our previous observations with $C_{30}H_{12}$ in terms of a charge-transfer transition.[27] Indeed, multiwavelength analysis for three separate titration experiments in each solvent consistently afforded satisfactory results for the 1:1 binding model only.[33] In particular, we obtained $\log K_{a,exp} = 3.19 \pm 0.02$, 2.9 ± 0.4, and 3.3 ± 0.2 in PhCl, $CHCl_3$, and THF, respectively.

More pronounced were the spectral changes noted during the titration of truxTTF versus $C_{38}H_{14}$, as shown in Figure 3b. Here, we observed a significant decrease in the intensity of the truxTTF absorption band at around 450 nm, accompanied by the increase of a broad band and a charge-transfer band in the 500–600 nm region, with concomitant formation of an isosbestic point at 490 nm. The isosbestic point is, however, buried upon addition of more than one equivalent of $C_{38}H_{14}$. Multiwavelength analysis afforded binding constants of $\log K_{a,exp} = 3.4 \pm 0.1$ and 3.5 ± 0.2 in PhCl and THF, respectively. As seen in Table 1, the theoretical values estimated for log K_a are in very good agreement with the experimental results, supporting the

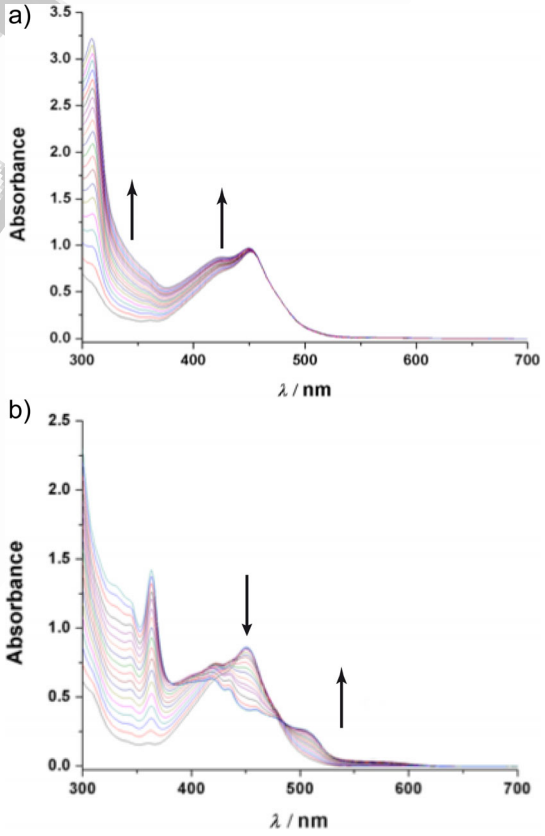

Figure 3. a) Experimental absorption spectra as obtained during the titration of truxTTF (1.76×10^{-4} M) with $C_{32}H_{12}$ (8.78×10^{-4} M) in PhCl at room temperature; up to 3.81 equivalents of $C_{32}H_{12}$ were added. b) Experimental absorption spectra as obtained during the titration of truxTTF (1.5×10^{-4} M) with $C_{38}H_{14}$ (7.7×10^{-4} M) in PhCl at room temperature; up to 3 equivalents of $C_{38}H_{14}$ were added.

formation of the staggered structures predicted theoretically as the preferred conformations.

Time-dependent DFT (TDDFT) calculations in the presence of the solvent (PhCl) were performed for the most stable structures of truxTTF·$C_{32}H_{12}$ (**4**) and truxTTF·$C_{38}H_{14}$ (**10**) and for their corresponding monomeric units, to disentangle the spectroscopic changes detected in the absorption spectra upon titration (see Supporting Information for computational details). TDDFT calculations on truxTTF·$C_{32}H_{12}$ predict four singlet excited states S_1–S_4 in the 500–650 nm range, with very low oscillator strengths ($f < 0.01$, Table S2, Supporting Information). These electronic transitions correspond to charge-transfer excitations from the HOMO and HOMO−1, located on truxTTF, to the LUMO and LUMO+1, located on $C_{32}H_{12}$ (Figure S3, Supporting Information), which relate to the hardly observed band recorded experimentally above 500 nm (Figure 3a). Similarly, the lowest singlet excited states S_1–S_4 for the truxTTF·$C_{38}H_{14}$ complex imply charge-transfer excitations, and are computed at 500–700 nm, with a moderate oscillator strength in the case of S_4 ($f = 0.016$). This state, in conjunction with the larger interaction energy, might explain the detection of the weak, broad CT band in the case of the $C_{38}H_{14}$-based dimer (Figure 3b). The new absorption band rising at 500 nm in truxTTF·$C_{38}H_{14}$ is assigned to the electronic transition to the first excited state S_1 of $C_{38}H_{14}$ calculated at 489 nm, which appears at a similar wavelength (492 nm) for truxTTF·$C_{38}H_{14}$ (Table S2). In contrast, $C_{32}H_{12}$ presents no significant absorption above 400 nm (Table S2† and Figure S4, Supporting Information). In both dimers, the typical truxTTF band centered at 450 nm is predicted to decrease slightly in intensity, but preserves its position upon complexation (Table S2† and Figure S5, Supporting Information). Finally, the experimental peak rising at 360 nm in truxTTF·$C_{38}H_{14}$ (Figure 3b) is assigned to the intense electronic transition to S_8 ($f = 0.373$) predicted for the $C_{38}H_{14}$ fragment at 356 nm. Spectroscopic changes in absorption upon complexation are therefore easily understood by joining the absorption features of the constituent monomeric units.

^{1}H NMR experiments helped to shed light on the structure of these associates in solution. Figure 4a shows the ^{1}H NMR spectra of truxTTF (black), $C_{32}H_{12}$ (blue), and truxTTF·$C_{32}H_{12}$ (red). The lettering is in accordance with Scheme 1 and shows the assignment for truxTTF. Upon complexation, all the signals of $C_{32}H_{12}$ suffer slight and quantitatively similar upfield shifts. Meanwhile, the signals corresponding to the truxene core of truxTTF (b–e in Figure 4) appear unaltered, and only the dithiole ring signals (a+a′ in Figure 4a) are shifted upfield by approximately 0.02 ppm. Moreover, a change in multiplicity from a singlet to two doublets ($J = 6.8$ Hz) with a very strong rooftop effect is also noticeable (see insets in Figure 4a). These changes support the structure depicted as **4** in Figure 1, which was calculated to be the only thermodynamically favorable arrangement in chloroform solution for truxTTF·$C_{32}H_{12}$ (vide supra).

The case of truxTTF·$C_{38}H_{14}$ is not so straightforward. The ^{1}H NMR spectra are shown in Figure 4b with analogous color coding. As in the previous example, all the signals of the corannulene-based buckybowls are shifted slightly upfield. However, we can see shielding of both the truxene core and the dithiole signals of truxTTF upon association. The former are quantitatively smaller and mostly affect the d and c triplets, whereas the latter are larger, and in this case do not result in a change of multiplicity, but only in broadening (see insets in Figure 4b). These spectroscopic changes point to a coexistence in solution of the staggered structures (**7**–**10** in Figure 2), with a predominance of those in which the dithiole rings are inside the cavity of $C_{38}H_{14}$ (**8** and **10** in Figure 2), again in perfect agreement with the relevant calculations.

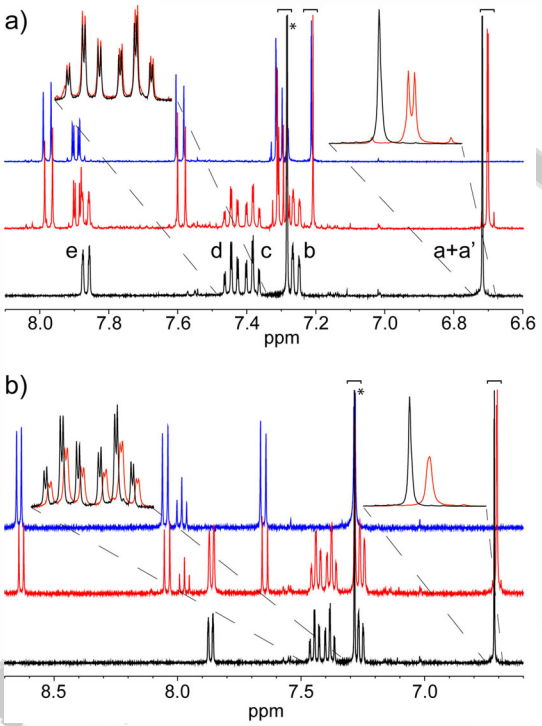

Figure 4. ^{1}H NMR spectra ($CDCl_3$, 400 MHz, 298 K, all species at ≈5 mM) of: a) truxTTF (black), $C_{32}H_{12}$ (blue), and truxTTF + $C_{32}H_{12}$ (red), and b) truxTTF (black), $C_{38}H_{14}$ (blue) and truxTTF + $C_{38}H_{14}$ (red). The insets show an overlay of the spectra of truxTTF and the complexes in the region 6.74–6.68 ppm (a+a′) and 7.48–7.34 ppm (c+d).

To shed light onto the excited state properties of truxTTF, $C_{38}H_{14}$, and their supramolecular associate truxTTF·$C_{38}H_{14}$, we conducted transient absorption experiments. Upon 480 nm excitation of truxTTF in chlorobenzene, a new transient develops immediately.[27] Characteristics of the latter are a marked maximum in the visible region at 530 nm, and marked ground-state bleaching observed around 450 nm. This excited state decays rapidly, as in other sulfur-rich electron donors, with a lifetime of only 1.0(±0.5) ps. This short lifetime is rationalized by the presence of the sulfur atoms, with strong second-order vibronic spin-orbit coupling, as it transforms into a much weaker absorbing state with maxima at 505 and 700 nm (Figure 5), with a detected lifetime of 20(±5) ps.

Upon excitation of $C_{38}H_{14}$ at 480 nm in chlorobenzene, several strong transient maxima evolve with the completion of the laser pulse (Figure 6). Three sharp maxima at 450, 546, and 800 nm are accompanied by broad transients ranging from 625 to 725 nm. After excitation, a multiexponential deactiva-

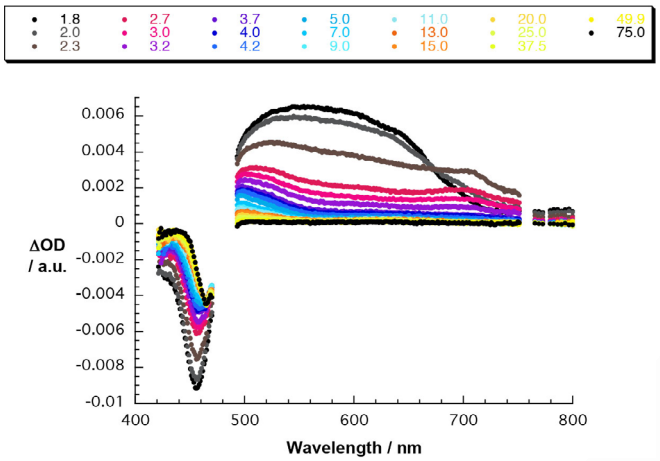

Figure 5. Differential absorption spectra obtained upon femtosecond pump probe experiments (480 nm) of truxTTF in argon-saturated chlorobenzene with time delays of 1.8–75 ps at room temperature.

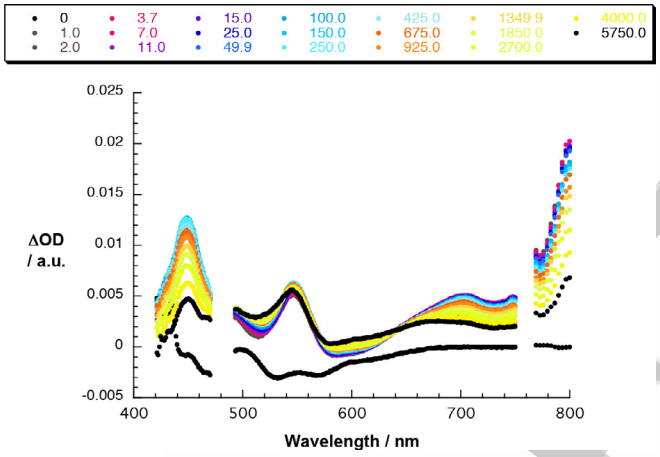

Figure 6. Differential absorption spectra obtained upon femtosecond pump probe experiments (480 nm) of $C_{38}H_{14}$ in argon-saturated chlorobenzene with time delays of 0–5750 ps at room temperature.

tion of these features is observed. Whereas the 546 nm maximum persists, the features at 450 and 800 nm and 625–725 nm deactivate within 46 ps (20%) and 3.5 ns (80%). The former is assigned to a nonradiative intrinsic deactivation, and the latter reflects the intersystem crossing to the triplet excited state of $C_{38}H_{14}$. The triplet excited state shows a transient absorption maximum at 546 nm and one broad transient around 670 nm, which deactivates within 18 μs to the ground state. Experiments in toluene and benzonitrile gave similar results.

To gain insight into the processes occurring after photoexcitation, we conducted spectroelectrochemical measurements, that is, we recorded the differential absorption spectra upon electrochemical oxidation of truxTTF[27] and reduction of $C_{38}H_{14}$ (Figure 7). TDDFT calculations were performed on the anion species of $C_{38}H_{14}$, and the simulated differential absorption spectrum is shown in Figure S7 (Supporting Information). The broad band, experimentally centered around 650 nm, corresponds to the $D_0 \rightarrow D_4$ excitation of $C_{38}H_{14}^{\bullet-}$ with oscillator strength $f = 0.094$. Theoretical calculations nicely reproduce the

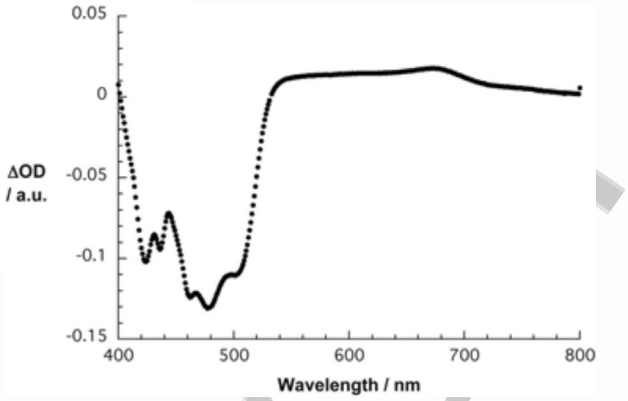

Figure 7. Differential absorption spectrum obtained upon electrochemical reduction of $C_{38}H_{14}$ in deoxygenated *ortho*-dichlorobenzene containing $TBAPF_6$ (0.1 M) with an applied potential of −1.1 V versus Ag wire at room temperature.

crossing point around 550 nm, that is, the negative signal at 500 nm originated by the intense S_1 excited state of neutral $C_{38}H_{14}$.

Upon excitation of truxTTF·$C_{38}H_{14}$ (10:1) in toluene, chlorobenzene, or benzonitrile at 480 nm, truxTTF-centered transients dominate the spectra (Figure 8) rather than charge-transfer-related characteristics.[34] In particular, the 530 nm marker is discernible at the conclusion of the excitation. With a lifetime of 0.8(±0.2) ps, the latter transforms into a new transient species, that is, the charge-separated state featuring truxTTF$^{\bullet+}$ and $C_{38}H_{14}^{\bullet-}$. Of great importance are changes in the differential absorption in the range between 500 and 700 nm, at which both the truxTTF$^{\bullet+}$ and the $C_{38}H_{14}^{\bullet-}$ species present higher absorption (Figure 7), supporting the notion of electronic communications taking place in the excited state.

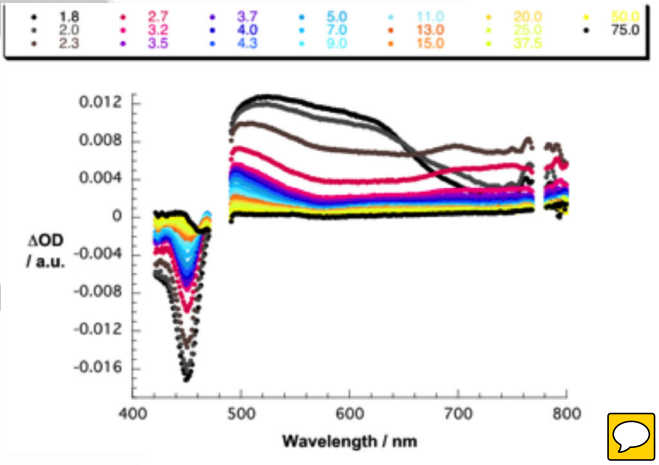

Figure 8. Differential absorption spectra obtained upon femtosecond pump probe experiments (480 nm) of truxTTF·$C_{38}H_{14}$ (10:1) in argon-saturated toluene with time delays of 1.8–75 ps at room temperature.

A detailed kinetic analysis corroborates our hypothesis. To this end, multiwavelength analysis yields four major lifetime components. After excitation, a very short lifetime of 0.8(±0.2) ps■■ok?■■ is followed by a 15(±5) ps component. We

assign the shorter component to ultrafast charge separation yielding the truxTTF$^{\bullet+}$·$C_{38}H_{14}^{\bullet-}$ charge-separated state. The longer component is probably attributable to intrinsic deactivation of noncomplexated truxTTF and $C_{38}H_{14}$. The third component of 160(±15) ps, which is observed neither for truxTTF nor for $C_{38}H_{14}$, reflects the charge recombination to yield truxTTF·$C_{38}H_{14}$ in the ground state. Finally, the fourth component of >5.5 ns is probably caused by the slow deactivation of the $C_{38}H_{14}$ triplet excited state, as confirmed by the detection of the 450, 546, and 800 nm markers. The latter is populated by intersystem crossing within noncomplexated $C_{38}H_{14}$ and, potentially, charge recombination.

Upon excitation of $C_{32}H_{12}$ at 500 nm in chlorobenzene, a transient centering at 520 nm is observed (Figure 9). This feature deactivates within 1.6 ns to the ground state or the lower-lying triplet excited state, which is, however, not observed spectroscopically. Similar results were observed in toluene, anisole, *ortho*-dichlorobenzene, and benzonitrile.

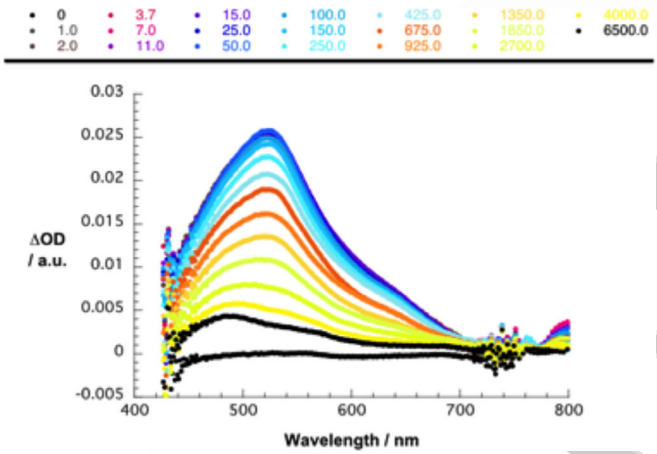

Figure 9. Differential absorption spectra obtained upon femtosecond pump probe experiments (500 nm) of $C_{32}H_{12}$ in argon-saturated chlorobenzene with time delays of 0–6500 ps at room temperature.

To shed light on the excited state interactions between truxTTF and $C_{32}H_{12}$, we explored mixtures of various molar ratios (10:1–1:10) in solvents of different polarities (anisole, toluene, chlorobenzene, *ortho*-dichlorobenzene, and benzonitrile) through transient absorption experiments with excitation at 387 and 480 nm. Figure 10 exemplifies the differential absorption changes recorded in chlorobenzene. The spectral similarity between the excited-state absorptions of truxTTF and $C_{32}H_{12}$, on one hand, and the radical cation of truxTTF as well as the radical anion of $C_{32}H_{12}$ (Figure 11), on the other hand, rendered an unambiguous characterization of the charge-separated state truxTTF$^{\bullet+}$·$C_{32}H_{12}^{\bullet-}$ rather difficult. TDDFT simulations confirmed the absence of any characteristic feature for the anion species of $C_{32}H_{12}$ above 700 nm (Figure S6, Supporting Information) that could help in identifying the charge-separated state. On the basis of the current investigation with $C_{38}H_{14}$ and the past investigation with $C_{30}H_{12}$, excited-state interactions in terms of charge transfer with truxTTF are likely to occur.[27]

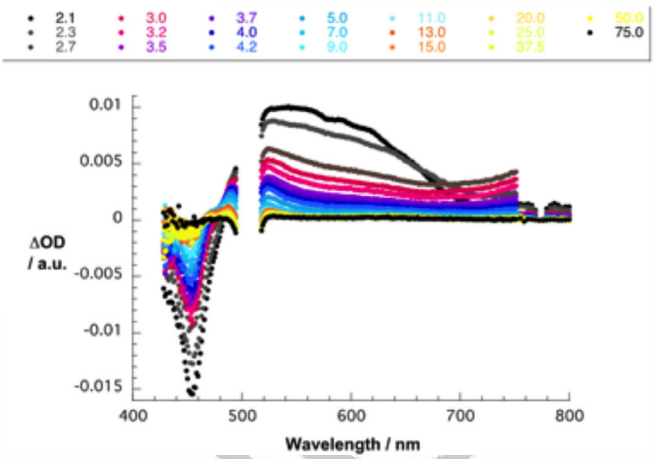

Figure 10. Differential absorption spectra obtained upon femtosecond pump probe experiments (500 nm) of truxTTF·$C_{32}H_{12}$ (10:1) in argon-saturated *ortho*-dichlorobenzene with time delays of 1.8–75 ps at room temperature.

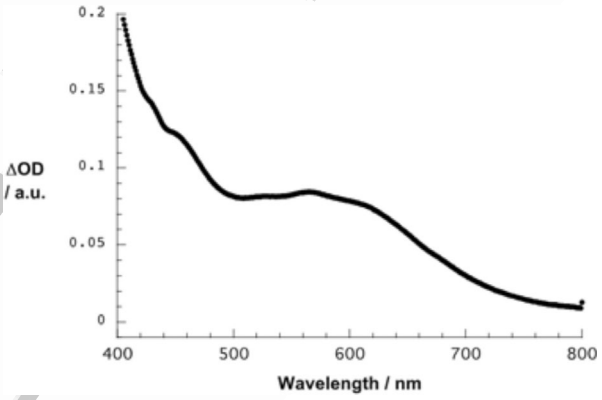

Figure 11. Differential absorption spectra obtained upon electrochemical reduction of $C_{32}H_{12}$ in deoxygenated *ortho*-dichlorobenzene containing $TBAPF_6$ (0.1 M) with an applied potential of −1.0 V versus Ag wire at room temperature.

Conclusions

We have demonstrated the association of two corannulene-based fullerene fragments, $C_{32}H_{12}$ and $C_{38}H_{14}$, with a bowl-shaped tetrathiafulvalene unit, truxTTF. Absorption titrations aided in following the complexation process. The most remarkable features are the depletion of intrinsic truxTTF absorption upon addition of $C_{32}H_{12}$ or $C_{38}H_{14}$, accompanied by the rise of a charge-transfer band in the visible region between 500 and 600 nm. Multiwavelength analysis revealed association constants of $\log K_a = 2.9–3.5$. DFT calculations performed at the revPBE0-D3/cc-pVTZ level supported the supramolecular association. Here, different possible complex geometries were predicted, revealing either bowl-in-bowl or staggered arrangements, with the latter offering the largest interaction energies, even surpassing the association energy obtained for the analogous truxTTF·$C_{30}H_{12}$ complex. Accurate calculations of the free energy of complexation suggested that only the staggered conformer in which one dithiole ring is placed inside the bowl

basin could be formed in solution for truxTTF·$C_{32}H_{12}$, whereas a mixture of staggered conformers might be present for truxTTF·$C_{38}H_{14}$. NMR experiments confirmed these theoretical predictions. Femtosecond transient absorption studies shed light on the excited-state interactions in the associates. In the case of truxTTF·$C_{38}H_{14}$, photoexcitation yielded the charge-separated state truxTTF$^{\bullet+}$·$C_{38}H_{14}^{\bullet-}$ with a lifetime of approximately 160 ps in the most polar solvent benzonitrile. For truxTTF·$C_{32}H_{12}$, the assignment of the charge-separated state was extremely difficult, but on the basis of earlier findings, its existence is regarded to be very likely.

These experimental and theoretical findings reveal π-extended corannulene derivatives as suitable systems to form 1:1 supramolecular complexes with bowl-shaped electron-donor molecules, in which intermolecular PET processes occur, mimicking the related buckyballs.

Acknowledgements

Financial support by the European Research Council (ERC-320441-Chiralcarbon and MINT, ERC-StG-307609), MINECO of Spain (CTQ2014-52045-R, CTQ2015-71154-P, CTQ2014-60541-P, and Unidad de Excelencia María de Maeztu MDM-2015-0538), the CAM (FOTOCARBON project S2013/MIT-2841), European Feder funds (CTQ2015-71154-P), and Generalitat Valenciana (PROMETEO/2016/135) is acknowledged. J.C. and M.G. thank the MECD of Spain for doctoral FPU grants. N.M. thanks the Alexander von Humboldt Foundation. D.M.G. gratefully acknowledges funding from the Deutsche Forschungsgemeinschaft as part of the Collaborative Research Centre SFB 953 "Synthetic Carbon Allotropes" and of the Excellence Cluster "Engineering of Advanced Materials". The Bayerische Staatsregierung is acknowledged for funding granted as part of the "Solar Technologies go Hybrid" initiative.

Keywords: association constants · buckybowls · donor–acceptor systems · photoinduced charge transfer · supramolecular chemistry

[1] A. Narita, X.-Y. Wang, X. Feng, K. Müllen, *Chem. Soc. Rev.* **2015**, *44*, 6616 – 6643.
[2] R. Rieger, K. Müllen, *J. Phys. Org. Chem.* **2010**, *23*, 315 – 325.
[3] J. Wu, W. Pisula, K. Müllen, *Chem. Rev.* **2007**, *107*, 718 – 747.
[4] M. Gingras, G. Felix, R. Peresutti, *Chem. Soc. Rev.* **2013**, *42*, 1007 – 1050.
[5] M. Gingras, *Chem. Soc. Rev.* **2013**, *42*, 968 – 1006.
[6] M. Gingras, *Chem. Soc. Rev.* **2013**, *42*, 1051 – 1095.
[7] E. R. Darzi, R. Jasti, *Chem. Soc. Rev.* **2015**, *44*, 6401 – 6410.
[8] J. Evans Paul, R. Darzi Evan, R. Jasti, *Nat. Chem.* **2014**, *6*, 404 – 408.
[9] T. Matsuno, S. Sato, R. Iizuka, H. Isobe, *Chem. Sci.* **2015**, *6*, 909 – 916.
[10] Y. Miyauchi, K. Johmoto, N. Yasuda, H. Uekusa, S. Fujii, M. Kiguchi, H. Ito, K. Itami, K. Tanaka, *Chem. Eur. J.* **2015**, *21*, 18900 – 18904.
[11] K. Kato, Y. Segawa, L. T. Scott, K. Itami, *Chem. Asian J.* **2015**, *10*, 1635 – 1639.
[12] *Fragments of Fullerenes and Carbon Nanotubes: Designed Synthesis Unusual Reactions, and Coordination Chemistry* (Eds.: M. A. Petrukhina, L. T. Scott) Wiley, **2012**.
[13] Y.-T. Wu, J. S. Siegel, *Top. Curr. Chem.* **2014**, *349*, 63 – 120.
[14] L. T. Scott, H. E. Bronstein, D. V. Preda, R. B. M. Ansems, M. S. Bratcher, S. Hagen, *Pure Appl. Chem.* **1999**, *71*, 209 – 219.
[15] L. T. Scott, M. S. Bratcher, S. Hagen, *J. Am. Chem. Soc.* **1996**, *118*, 8743 – 8744.
[16] E. E. Maroto, A. de Cozar, S. Filippone, A. Martín-Domenech, M. Suarez, F. P. Cossío, N. Martín, *Angew. Chem. Int. Ed.* **2011**, *50*, 6060 – 6064; *Angew. Chem.* **2011**, *123*, 6184 – 6188.
[17] M. A. Petrukhina, L. T. Scott, *Dalton Trans.* **2005**, 2969 – 2975.
[18] P. A. Vecchi, C. M. Alvarez, A. Ellern, R. J. Angelici, A. Sygula, R. Sygula, P. W. Rabideau, *Angew. Chem. Int. Ed.* **2004**, *43*, 4497 – 4500; *Angew. Chem.* **2004**, *116*, 4597 – 4600.
[19] T. Amaya, H. Sakane, T. Hirao, *Angew. Chem. Int. Ed.* **2007**, *46*, 8376 – 8379; *Angew. Chem.* **2007**, *119*, 8528 – 8531.
[20] U. H. F. Bunz, S. Menning, N. Martín, *Angew. Chem. Int. Ed.* **2012**, *51*, 7094 – 7101; *Angew. Chem.* **2012**, *124*, 7202 – 7209.
[21] L. T. Scott, E. A. Jackson, Q. Zhang, B. D. Steinberg, M. Bancu, B. Li, *J. Am. Chem. Soc.* **2012**, *134*, 107 – 110.
[22] K. Müllen, J. P. Rabe, *Acc. Chem. Res.* **2008**, *41*, 511 – 520.
[23] J. Wu, W. Pisula, K. Müllen, *Chem. Rev.* **2007**, *107*, 718 – 747■■Duplicate of [3]; please remove/replace & renumber■■
[24] T. Kawase, H. Kurata, *Chem. Rev.* **2006**, *106*, 5[illegible]6273.
[25] E. M. Pérez, N. Martín, *Chem. Soc. Rev.* **2008**, *37*, 1512 – 1519.
[26] E. M. Pérez, N. Martín, *Chem. Soc. Rev.* **2015**, *44*, 6425 – 6433.
[27] M. Gallego, J. Calbo, J. Aragó, R. M. Krick Calderon, F. H. Liquido, T. Iwamoto, A. K. Greene, E. A. Jackson, E. M. Pérez, E. Ortí, D. M. Guldi, L. T. Scott, N. Martín, *Angew. Chem. Int. Ed.* **2014**, *53*, 2170 – 2175; *Angew. Chem.* **2014**, *126*, 2202 – 2207.
[28] M.-K. Chen, H.-J. Hsin, T.-C. Wu, B.-Y. Kang, Y.-W. Lee, M.-Y. Kuo, Y.-T. Wu, *Chem. Eur. J.* **2014**, *20*, 598 – 608.
[29] T.-C. Wu, M.-K. Chen, Y.-W. Lee, M.-Y. Kuo, Y.-T. Wu, *Angew. Chem. Int. Ed.* **2013**, *52*, 1289 – 1293; *Angew. Chem.* **2013**, *125*, 1327 – 1331.
[30] E. M. Pérez, M. Sierra, L. Sánchez, M. R. Torres, R. Viruela, P. M. Viruela, E. Ortí, N. Martín, *Angew. Chem. Int. Ed.* **2007**, *46*, 1847 – 1851; *Angew. Chem.* **2007**, *119*, 1879 – 1883.
[31] T.-C. Wu, H.-J. Hsin, M.-Y. Kuo, C.-H. Li, Y.-T. Wu, *J. Am. Chem. Soc.* **2011**, *133*, 16319 – 16321.
[32] M. A. Petrukhina, K. W. Andreini, L. Peng, L. T. Scott, *Angew. Chem. Int. Ed.* **2004**, *43*, 5477 – 5481; *Angew. Chem.* **2004**, *116*, 5593 – 5597.
[33] Multiwavelength analysis testing several binding models is the most accurate way of determining stoichiometry. Job plots have been shown to fail for most host–guest systems and conditions. See: a) D. Brynn Hibbert, P. Thordarson, *Chem. Commun.* **2016**, *52*, 12792 – 12805; b) P. Thordarson, *Chem. Soc. Rev.* **2011**, *40*, 1305 – 1323.
[34] The presence of the latter cannot be ruled out, but it is likely that fast vibrational deactivation limits its detection.
[35] Experiments with excitation into the charge-transfer transition, that is, in the 500–600 nm region, were hampered by low extinction/oscillator strength.

Manuscript received: October 21, 2016
Accepted Article published: January 11, 2017
Final Article published: ■■ ■■, 0000

FULL PAPER

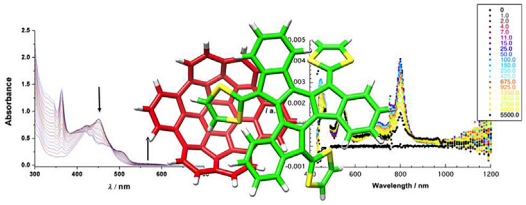

Pitch a curve: The association behavior of a bowl-shaped, truxene-based tetrathiafulvalene (truxTTF) with corannulene-based fullerene fragments is investigated. These π-extended corannulene derivatives are revealed to be suitable systems for the formation of 1:1 supramolecular complexes with bowl-shaped electron-donor molecules, in which intermolecular photoinduced electron transfer occurs, mimicking the related buckyballs (see figure).

Supramolecular Chemistry

M. Gallego, J. Calbo, R. M. Krick Calderon, P. Pla, Y.-C. Hsieh, E. M. Pérez, Y.-T. Wu, E. Ortí,* D. M. Guldi,* N. Martín**

■■ – ■■

Complexation and Electronic Communication between Corannulene-Based Buckybowls and a Curved Truxene-TTF Donor

Please check that the ORCID identifiers listed below are correct. We encourage all authors to provide an ORCID identifier for each coauthor. ORCID is a registry that provides researchers with a unique digital identifier. Some funding agencies recommend or even require the inclusion of ORCID IDs in all published articles, and authors should consult their funding agency guidelines for details. Registration is easy and free; for further information, see http://orcid.org/.

Dr. María Gallego
Joaquín Calbo
Dr. Rafael M. Krick Calderon
Paula Pla
Dr. Ya-Chu Hsieh
Dr. Emilio M. Pérez http://orcid.org/0000-0002-8739-2777
Prof. Dr. Yao-Ting Wu
Prof. Dr. Enrique Ortí
Prof. Dr. Dirk M. Guldi
Prof. Dr. Nazario Martín